Tunnelling and Underground Space Technology 51 (2016) 202–211

Contents lists available at ScienceDirect

Tunnelling and Underground Space Technology

journal homepage: www.elsevier.com/locate/tust

Full waveform inversion applied in defect investigation for ballastless undertrack structure of high-speed railway

Huan Wang, Ailan Che *, Shaokong Feng, Xiurun Ge

School of Naval Architecture, Ocean and Civil Engineering, Shanghai Jiaotong University, 800 Dongchuan-Road, Shanghai 200240, China

ARTICLE INFO

Article history:
Received 26 September 2014
Received in revised form 21 May 2015
Accepted 19 October 2015

Keywords:
High-speed railway
Ballastless undertrack structure
FWI method
Low-velocity layers
Quantitative investigation

ABSTRACT

Until the end of 2015, China will build a national high-speed railway network with total mileage of exceed 20,000 km. The Ballastless undertrack structure is wildly used in this network. Filed investigation shows that the damage and defects in ballastless undertrack structure will grow by long-term dynamic loading during the operation and bring potential risk to the operation safety. For better characterization of these internal problems, a time-domain full waveform inversion (FWI) method based on quasi-linear method and random search algorithm is developed as nondestructive testing (NDT) method. Tikhonov regularization is adopted to alleviate the ill conditioned matrix. Also, cross convolutions between observed data and forward response waveforms are employed to allow this FWI method to get rid of the influence of the source. According to filed investigation, two numerical case studies considered with horizontal discontinuity of material are carried out. It is verified that the presented technical is capable for characterizing anomalies of various zones in buried low-velocity layers. Meanwhile the FWI method is applied to experimental data in a real full scale model of ballastless high-speed railway undertrack structure. The inversion work successfully reveals the preset defects and damages inside the CA mortar layer and embankment. The results are generally consistent with the preset model.

1. Introduction

As part of its rapid urbanization efforts, China has spent billions of dollars over the last decade on building a national high-speed railway network. Until the end of 2015, there will be 42 high-speed passenger railway lines built and operated. At that time, its total mileage will exceed 20,000 km (Wang, 2005). But during the operation, it is found that the damage and defects will be generated in the high-speed railway undertrack structure under the long-term dynamic loading from locomotive. What is more, the damage and defects will be grown and bring potential risk to the operation safety. As a result, the detection methods to reveal internal problems, especially the nondestructive testing (NDT) method, have been attracting more and more attention.

Generally, most of the high-speed railways are operated on ballastless track and its undertrack structure contains four parts (from top to bottom): track slab, cement asphalt (CA) mortar, support plate and embankment, as shown in Fig. 1. The track slab and support plate are made of reinforced concrete and the embankment is built by dense-graded stone asphalt mixtures, Because the strengths of CA mortar and embankment are relatively weak, damage and defects are mainly concentrated on this two layers, such as separation, void, permeation and cracks (Yang and Gao, 2004).

The defect investigation on ballastless high-speed railway undertrack structure can be regarded as a process of revealing the soft sandwich layer with low S-wave velocity. Many traditional geotechnical methods has been used, such as the travel time methods using arrival signals of wave components (Song et al., 2003), the surface wave methods involving wave velocity dispersion (Feng et al., 2009) and the ground penetrating radar (GPR) methods based on the reflection of electromagnetic wave (Cassidy and Millington, 2009). It is reported that the low-velocity regions are not well characterized by travel time methods since the medium contrasts are approximated as gradient regions (Sheehan et al., 2005). Also, in the case of shear wave velocity reversals and high stiffness contrasts, the higher modes will get more energy and become dominant in wave velocity dispersion, as a result, the information of strata below low-velocity layers cannot be well revealed by surface wave methods (O'Neill et al., 2003). For the track slab is built with high reinforcement density, the GPR methods will be greatly restricted by the electromagnetic wave shield. Moreover, the GPR methods have some limitations in required quantitative evaluations because of the insensitivity to elastic parameters like elastic modulus and Poisson ratio (Xu et al., 2006).

* Corresponding author.
E-mail address: alche@sjtu.edu.cn (A. Che).

http://dx.doi.org/10.1016/j.tust.2015.10.035
0886-7798/

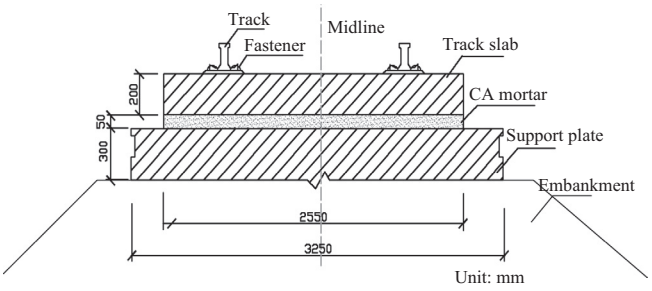

Fig. 1. Sketch of ballastless high-speed railway undertrack structure.

Many studies show that the full waveform inversion (FWI) method is capable of characterizing anomalies of low- and high-velocity zones (Virieux and Operto, 2009; Tran and McVay, 2012). It offers higher resolution of target medium and feasibility for the detection on buried low-velocity layers, so it is potential for quantitative investigation on high-speed railway undertrack structure. The FWI method grasps property information from received response waveforms and it is available for various elastic parameters of underground medium. It iteratively improves an initial model of the subsurface by fitting the observed with modeled data (Bunks et al., 1995; Brossier et al., 2009). However, as a computationally demanding task, the application of FWI method in geotechnical engineering is still in start-up and there are still obstacles to its full solution, such as the presence of ill-posedness and dependency on initial model. Many algorithms have been developed for overcoming above obstacles. Sheen et al. (2006) introduced reciprocity principle and convolution theorem for calculating partial derivatives explicitly, resulting in a significant decrease on the amounts of memory and computation for Jaccobian and approximate Hessian matrices. Romdhane et al. (2011) performed a full-waveform inversion algorithm involving both body and surface waves for near-surface investigation on a small scale model.

Herein, the framework of full waveform inversion method used in high-speed railway undertrack structure mainly contained two critical issues: the forward computation and inversion approach. In forward computation, accurate response waveforms in an undertrack structure model are generated by solving the elastic wave equation. In the inversion process, the initial model of internal structure iteratively improved by systematic fitting to the observed data. A time-domain full-waveform inversion algorithm based on a quasi-linear method (Crase et al., 1992) coupled with the random search algorithm (Huang and Kelkar, 1996; Brigham and Aquino, 2007) is developed for the revealing work of high-speed railway undertrack structure. Assume that the prior information is sufficient and the undertrack structure is simplified as a two-dimensional model. Two case studies, in which the damage and defects are mainly occurred in the layers of CA mortar and embankment, are carried out. The parameters to be extracted are concentrated on the S-wave velocities of distinguished regions in buried low-velocity layers. Besides that, in order to verify the resistance on noise, the noise-corrupted analysis is worked out. Based on numerical results, the FWI method is applied to real data from a full scale model of ballastless high-speed railway undertrack structure. Some artificial damage and defects are buried in CA mortar layer and embankment of undertrack structure respectively. The field tests including excitation and data acquisition are carried out on the surface of track slab. Before the inversion work, pretreatments including filtering and normalization are imposed on the field waveforms. Finally, the inversion work quantitatively reveals the defect and damages inside the CA mortar and embankment layer in undertrack structure.

2. Methodology

2.1. Forward modeling

The forward modeling is process of solving the elastic wave propagation equations by finite-difference time domain (FDTD) method. Two-dimensional elastic wave propagation is described by a set of the second-order linear partial differential equations as follows:

Navier equation in which body forces are ignored

$$\begin{cases} \rho \frac{\partial^2 u_x}{\partial t^2} = (\lambda + 2\mu)\frac{\partial^2 u_x}{\partial x^2} + (\lambda + \mu)\frac{\partial^2 u_z}{\partial x \partial z} + \mu \frac{\partial^2 u_x}{\partial z^2} \\ \rho \frac{\partial^2 u_z}{\partial t^2} = (\lambda + 2\mu)\frac{\partial^2 u_z}{\partial z^2} + (\lambda + \mu)\frac{\partial^2 u_x}{\partial x \partial z} + \mu \frac{\partial^2 u_z}{\partial x^2} \end{cases} \quad (1)$$

where (u_x, u_z) is the particle displacement vector, ρ is the mass density and λ, μ are the Lame' coefficients. At the source locations, the medium is perturbed as enforced displacement.

Because the inversion results are generated by fitting the observed data to responded waveforms estimated by forward modeling, it is important to accurately model the responded waveforms, so the finite-difference time domain (FDTD) method (Smith, 1985) is adopted. Meanwhile, the perfectly matched layer (PML) method (Berenger, 1994; Chew and Liu, 1996) is employed as absorbing boundary condition. The code is developed in Matlaband all displacements are calculated in matrix format and processed at each time step.

2.2. Inversion approach

The inversion work can be considered as an optimization process minimizing the residual between the observed data and forward response waveforms. The residual is usually measured by a least-squares error criterion as

$$Q = \|\boldsymbol{\varepsilon}\|_2 = \|\boldsymbol{F}(\boldsymbol{x}) - \boldsymbol{F}^{\text{obs}}\|_2 \quad (2)$$

where $\|\ \|_2$ denotes the L2-norm, Q is an objective function for the optimization process; $\boldsymbol{\varepsilon}$ is residual waveforms; $\boldsymbol{F}^{\text{obs}}$ and $\boldsymbol{F}(\boldsymbol{x})$ are observed data and forward response waveforms respectively; vector $\boldsymbol{x}$ is parameter vector of simplified model which is described as

$$\boldsymbol{x} = (x_1, x_2, \ldots, x_n)^T$$

where subscript numbers denote the target parameters in inversion respectively; n is the number of parameters to be extracted and T denotes the transpose.

To avoid influence of the source on the inversion work, the residual matrix $\boldsymbol{\varepsilon}$ is modified using cross-convolved waveforms (Cheong et al., 2006). In details, the forward response waveforms are convolved with a reference trace from the observed data while the observed data are convolved with a reference trace from the forward response waveforms. Here, we select the first trace as the reference trace because of its relatively higher quality in site. Thus the objective function is modified as

$$Q = \|\boldsymbol{\varepsilon}\|_2 = \|\boldsymbol{F}_j(\boldsymbol{x}) * \boldsymbol{F}_1^{\text{obs}} - \boldsymbol{F}_j^{\text{obs}} * \boldsymbol{F}_1(\boldsymbol{x})\|_2 \quad (3)$$

where the subscript numbers denote the jth trace and the symbol '*' denotes the convolution.

At the start of inversion, an initial parameter vector $\boldsymbol{x}^0$ is established by prior information, such as geotechnical investigation, parameter scales and design plan. Then the objective function Q is minimized by updating parameter vector $\boldsymbol{x}$ by Quasi-linear method. The parameter vector $\boldsymbol{x}$ in $(n+1)$th iteration is obtained by

$$\boldsymbol{x}^{n+1} = \boldsymbol{x}^n + (\boldsymbol{J} + a\boldsymbol{E})^{-1}\boldsymbol{B} \quad (4)$$

where $\boldsymbol{E}$ is identity matrix. $\boldsymbol{J}$ is the Jacobian matrix, which can be obtained by taking the partial derivatives of forward response

waveforms with respect to parameter vector $\boldsymbol{x}$ and convolved with the reference trace. And $\boldsymbol{B}$ is a coefficient vector related to the residual matrix $\boldsymbol{\varepsilon}$. The Jacobian matrix $\boldsymbol{J}$ and coefficient vector $\boldsymbol{B}$ are expressed by Eqs. (5) and (6) respectively. And a is Tikhonov regularization parameter (Lampe and Voss, 2013) and determined by Eq. (7) in each iteration.

$$J_{p,l} = \sum_{j=2}^{m}\left[\left(\frac{\partial \boldsymbol{F}_j(\boldsymbol{x})}{\partial x_p} * \boldsymbol{F}_1^{\text{obs}}\right)\cdot\left(\frac{\partial \boldsymbol{F}_j(\boldsymbol{x})}{\partial x_l} * \boldsymbol{F}_1^{\text{obs}}\right)\right], \quad (p,l = 1,2,3,\ldots,n) \tag{5}$$

$$B_p = \sum_{j=2}^{m}\left[\left(\frac{\partial \boldsymbol{F}_j(\boldsymbol{x})}{\partial x_p} * \boldsymbol{F}_1^{\text{obs}}\right)\cdot \boldsymbol{\varepsilon}_j\right], \quad (p = 1,2,3,\ldots,n) \tag{6}$$

where m is the number of seismic traces and '·' is dot operator.

$$\alpha^{k+1} = (1/2)^k T_k^{\max} \tag{7}$$

where k is the iteration time, $T_k^{\max}$ is the maximum eigenvalue of Jacobian matrix $\boldsymbol{J}$ in kth iteration.

For a given observed data matrix $\boldsymbol{F}^{\text{obs}}$, there exits an appropriate parameter vector $\boldsymbol{x}$ (global minimum) which makes the forward response waveforms as close as to the observed data. Generally, as a kind of non-heuristic algorithm, the quasi-linear method has advantages in finite iteration steps, considerable calculate speed and relatively accurate solution, but its results and convergence are highly dependent on initial parameter vector $\boldsymbol{x}$ and easily trapped in local minima, which leads to improbable solution (Fu and Han, 2004; Yamanaka, 2005). So we adopt random search algorithm (RSA) coupled with the quasi-linear method to mitigate the disadvantages.

At first, a parameter vector $\boldsymbol{x}$ is reached by quasi-linear method, then check it whether belonging to local minimum point. If not, RSA is used for finding a new suitable initial parameter vector for quasi-linear method. The new vector $\boldsymbol{x}$ is searched by following equation:

$$x_{\text{new},i} = x_{\text{old},i} + (\text{sign}) \times \text{d}x_i \times \text{rand}, \tag{8}$$

where $x_{\text{new},i}$ and $x_{\text{old},i}$ are the new and unmodified ith parameter respectively; 'sign' is search direction and equals to 1 or −1 with half probability; $\text{d}x_i$ is search radius of each parameter and determined by prior information and empirical estimation. 'Rand' is a random number within the range of [0, 1].

During the search process of RSA method, if the value of objective function Q decreased, the temporary vector $\boldsymbol{x}$ is taken as a new initial parameter vector x for quasi-linear method. Repeat above steps several times until the terminal condition is satisfied and output the last parameter vector as global minimum results.

The steps of iteration of our full waveform inversion method are detailed, as shown in Fig. 2.

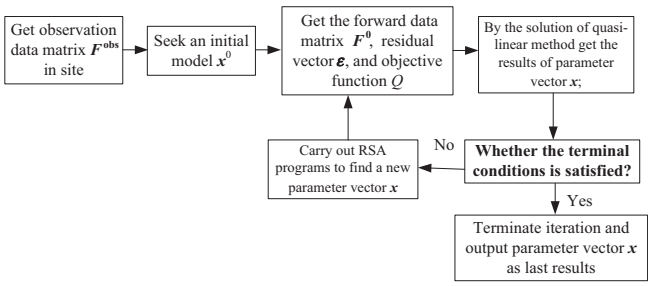

Fig. 2. The flow chart of iteration steps of full waveform inversion.

3. Numerical cases

3.1. Modeling

According to the filed investigation on a ballastless high-speed railway undertrack structure, we simplify it as a two-dimensional model in numerical case, as shown in Fig. 3. The first layer and third layer are set as concrete. The second layer between the track slab and the support plate is CA mortar. The rest of layers are embankments made by dense-graded stone asphalt mixtures. The physical property parameters of each material are listed in Table 1, where ρ and v_s are the density and S-wave velocity respectively and μ is the Poisson's ratio.

Since the damage and defects are mainly concentrated in the layers of CA mortar and embankment, the parameters of concrete are set as known in inversion and the target parameters to be extracted are concentrated on buried low-velocity layers. In view of the horizontal material discontinuity of the buried low-velocity layers, they are distinguished by some different regions, where the S-wave velocity of each region is to be solved, as shown in Fig. 3 (take the numerical case 1 as example, damage and defects are concentrated in CA mortar).

The numerical model in the FDTD forward computation is consisted of nearly 1920 nodes spaced 0.05 m vertically and horizontally. The Perfect Matched Layer (PML) absorbing boundary is applied on the left, right and bottom boundary of numerical model while the boundary condition on top is set as free. Since the S-wave velocity v_s can be determined by P-wave velocity v_p and Poisson's ratio and the mesh size Δl are predefined according to inverse resolution, the proper time step Δt here is considered by maximum P-wave velocity of the model. For that the maximum P-wave velocity in medium reaches nearly 4000 m/s, the step of finite difference is took as 5 μs to satisfy the differential stability conditions.

3.2. Inversion analysis

At the start of numerical analysis, a known S-wave velocity structure with a set of hypocenter and receivers is established,

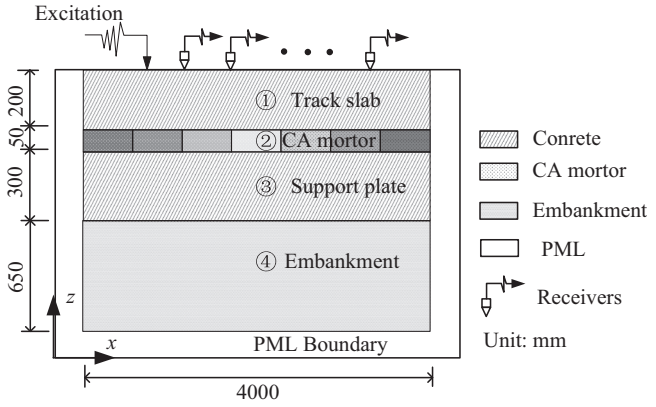

Fig. 3. Simplified two-dimensional model of high-speed railway undertrack structure.

Table 1
Material parameters in two-dimensional stratified model.

Materials	ρ (kg/m^3)	v_s (m/s)	μ
Concrete	2400	2200	0.2
CA mortor	1600	1500	0.3
Embankments	2300	1800	0.25

and the response waveforms on surface are obtained by forward computation. Then this response waveforms data is put into the inversion as observed data similar with the data acquired in field detection. At last the model of undertrack structure is revealed from this observed data. Theoretically, the final results should be the same as the model assumed before.

Similar with hammer sources used in field test, the excitation for observed data is an artificial signal which covers the most of frequency spectrums of various hammer sources. The waveform of artificial signal in time domain and its frequency spectrum within 0.1–4 kHz are shown in Fig. 4. As our inversion method is source independent, the source signature used for inversion is selected as Ricker wavelet with the central frequency of 2 kHz, as shown in Fig. 5.

The excitation is inputted at the upper free boundary vertically and response waveforms of vertical displacements on surface are recorded from m seismic receivers spaced every 0.25 m. And then the devices are moved forward at distance of Δd and above-mentioned processes are repeated until the whole measure line is finished, as Fig. 6 shows.

3.2.1. Case1: Damage and defects in CA mortar

According to the site investigation and long-term observation, when damage and defects exist in CA mortar, two common failure forms are found. The one is that CA mortar is damaged by long-term dynamic load and defect areas are generated where the bearing capacity is significantly declined. The other one is that considerable spaces are generated between CA mortar and track slab, which have the danger of expansion, as shown in Fig. 7. Here, in any forms, we assume that the layer of CA mortar is distinguished by 12 different regions with every width of 0.25 m (equal to the interval of seismic receivers). Two parts of damaged region are set in CA mortar and the S-wave velocity of damaged region is reduced to 750 m/s (half of the sound velocity). The correct structure of model is shown in Fig. 8(a).

In this numerical case, we use 8 seismic receivers for each excitation and the move step Δd = 0.5 m. The length of measure line is 3.5 m. 3 times of excitation are carried out. At the beginning of inversion, the initial S-wave velocities of CA mortar layer to be inversed are all set as 1100 m/s, as shown in Fig. 8(b).

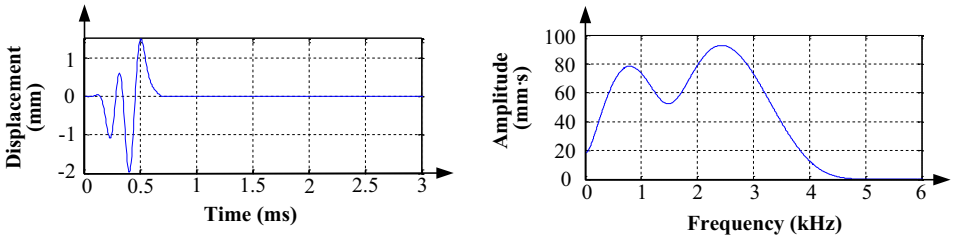

(a) Waveform in time domain (b) Frequency spectrum

Fig. 4. Artificial signal for observation data simulation.

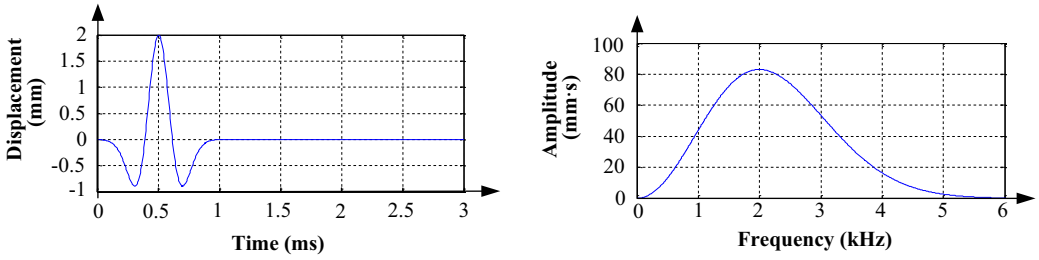

(a) Waveform in time domain (b) Frequency spectrum

Fig. 5. Ricker wavelet for inversion.

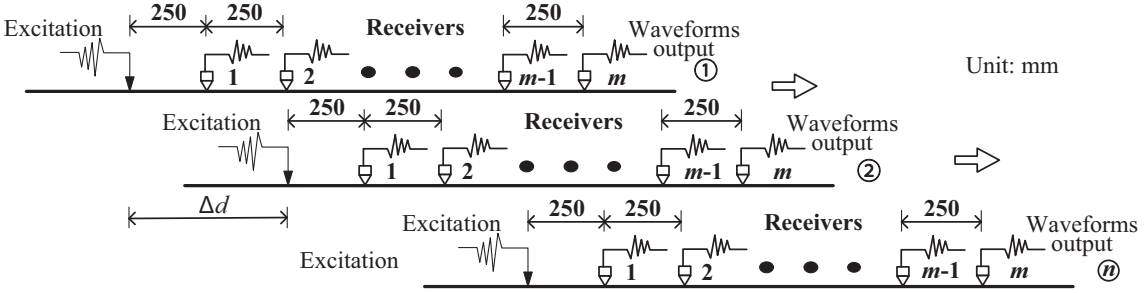

Fig. 6. Detection method on a measure line.

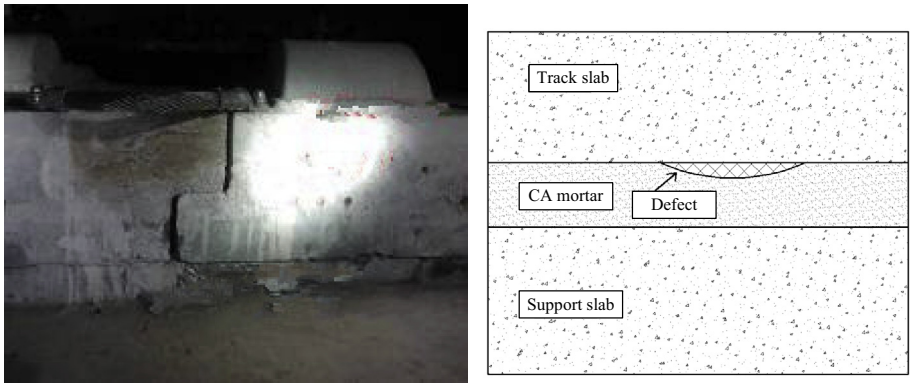

Fig. 7. Failure forms of CA mortar.

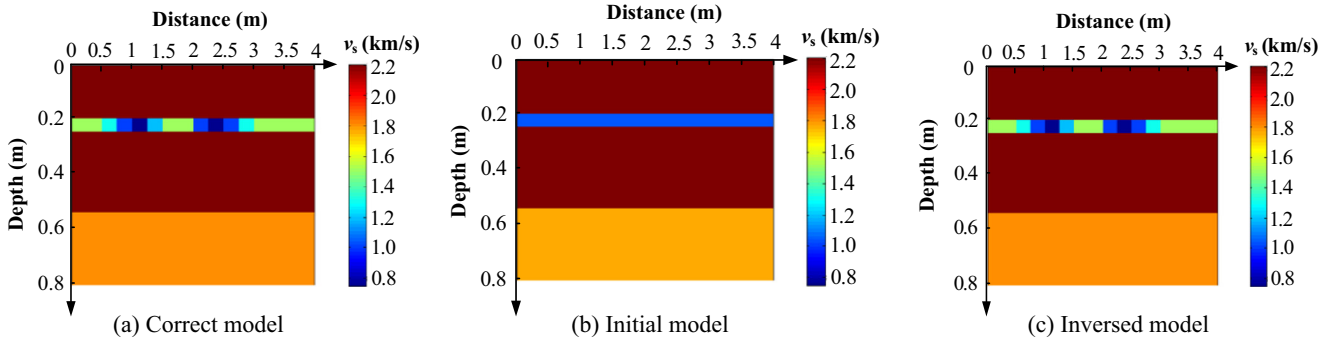

Fig. 8. Comparison of between correct model, initial model and inversed model in Case1.

As the inverse calculation is carried out, the model is improved by iterations. As expected, the normalized values of objective function are reduced quickly from 1.0 to 0.001 by 21 iterations. The values for iterations are presented in Fig. 9. The Final results are shown in Fig. 8(c). It is observed that the preset damage regions in CA mortar are clearly revealed and the results of inversed S-wave velocity structure agree well with the correct model. In view of the values of S-wave velocity, the maximum relative error was less than 3%.

3.2.2. Case2: Damage and defects in embankment

According to the site investigation and long-term observation, when damage and defects are generated in embankment, also several types of failure forms are found in the filed investigation as shown in Fig. 10. Firstly, because of the separation between embankment and support plate, water will be absorbed into the gap by dynamic load. As time passes, obvious damaged areas are generated in the embankment. Secondly, parts of soft foundation leaded the overlying embankment to be slightly sagging in operation and different settlements are occurred there as a result. Thirdly, its own disadvantages, such as crack and leakiness, are grown, enlarged, and come into considerable defects due to the dynamic load.

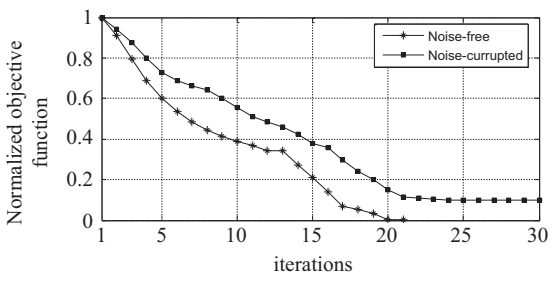

Fig. 9. Normalized values of objective function vary with iterations in Case1.

Similar with numerical case of CA mortar, the layer of embankment is distinguished by different regions, where the S-wave velocity of damaged region is reduced to 600 m/s (one third of the sound velocity). Otherwise, according to filed investigation, the damage and defects are only spread in the embankment within the depth of 0.25 m. So under the spread depth, the embankment is assumed as well. The correct structure in this numerical case is shown in Fig. 11(a).

The data acquisition, measure line and excitations are all same with the case of CA mortar. At the beginning of inversion, the initial S-wave velocities of embankment layer to be inversed are all set as 1100 m/s, as shown in Fig. 11(b). When the inverse calculation finished, the normalized values of objective function are reduced quickly from 1.0 to 0.003 by 25 iterations. The values for iterations are presented in Fig. 12. The Final results are shown in Fig. 11(c). The preset damage regions in embankment can also be clearly revealed and agree well with the correct model. The maximum relative error of inversed S-wave velocity is less than 3%.

3.3. Noise-corrupted analysis

In the noise-corrupted analysis, random noise with amplitude of 5% the peak observed data is plus on the waveforms. Then the inversion work is carried out again. For each numerical case, the normalized values of objective function are reduced and presented in Figs. 9 and 12 respectively. The iterations are terminated while the objective function approaches a certain value. The Final S-wave velocity structures with noise-corrupt are close to the results in

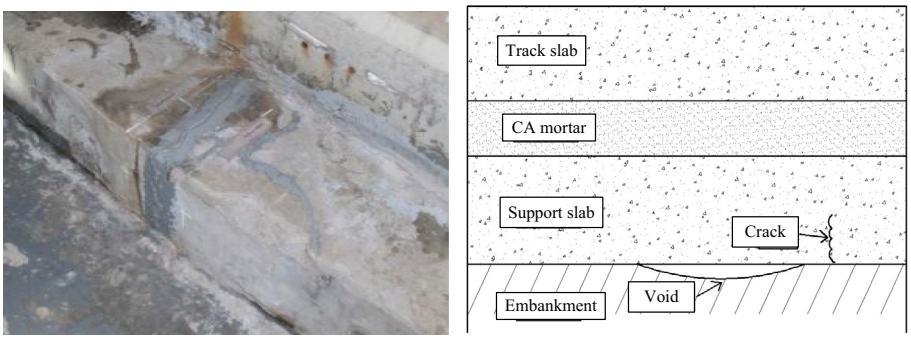

Fig. 10. Failure forms of embankment.

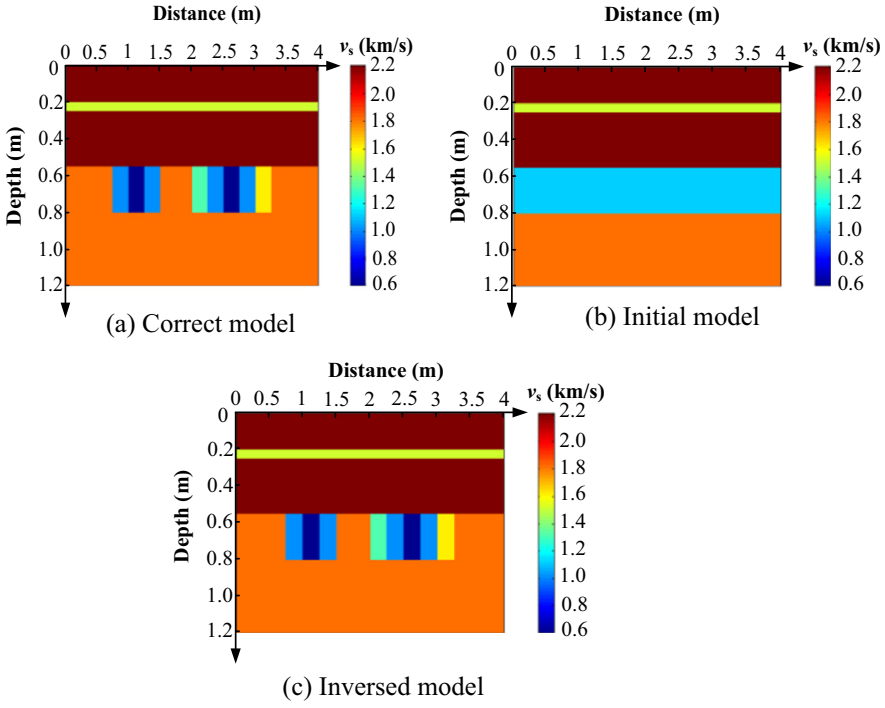

Fig. 11. Comparison of between correct model, initial model and inversed model in Case2.

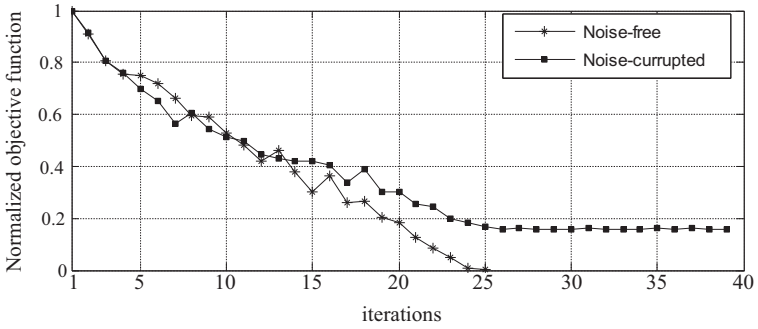

Fig. 12. Normalized values of objective function vary with iterations in Case2.

free-noise condition and the maximum relative error of inversed S-wave velocity only declines to near 11%. The comparison between initial and final residual data, which are convolved with corresponding reference trace, are presented in Fig. 13. Their residuals are significantly declined. It is verified that the affect from 5% random noise on the inversion work is not considerable and our

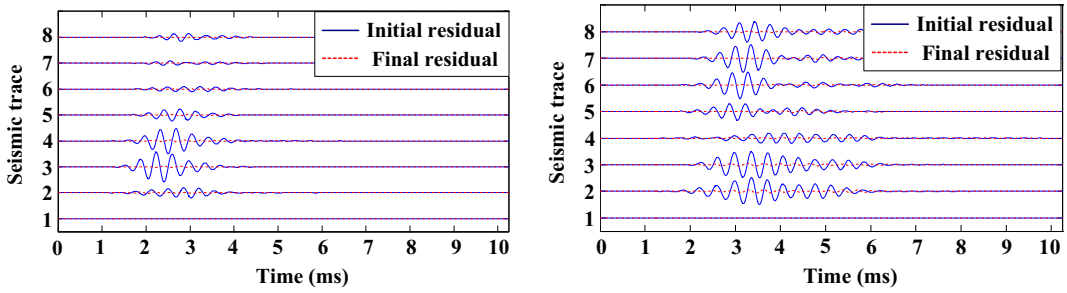

(a) Numerical case of CA mortor (b) Numerical case of embankment

Fig. 13. Comparison between initial and final convolved residual data in numerical simulation.

FWI method has certain of resistance on noise. But, considered the complexity and various factors, it is suggested that suitable noise filtering is still required before inversion work.

4. Applications on field model detection

In this section, the FWI method was applied to experimental data in a real full scale model of ballastless high-speed railway undertrack structure. In this model some defects were preset in layers of CA mortar and embankment.

4.1. General

The full scale model of high-speed railway was located in an experimental district of Shijiazhuang Railway Institute. The real model was built according with the present China CRTS-2 National Standard of ballastless high-speed railway undertrack structure, as shown in Fig. 14. The total length was 26.2 m and the width is 3.65 m.

Similar with the numerical cases, two types of defects were buried in CA mortar and embankment respectively, as shown in Fig. 15. The first one was void between CA mortar and track slab. In the void, the CA mortar was replaced by soft soil. Its shape was rectangular with size of $0.6 * 1.2\ m^2$ and its thickness was 0.05 m. The second one was weak area in embankment, where soft soil was full filled and its shape was round with diameter of 0.5 m and with depth of 0.25 m. The soft soil used in model was made by saturated surface soil.

4.2. Data acquisition and modeling

Because of the tracks and fasteners, the detecting area was concentrated near the midline, as shown in Fig. 15. In this detecting area, 3 measurement lines were arranged, whose length were 3.5 m. The process of waveform acquisition work on each measurement line was similar with the detection sketch in Fig. 6. Here, for one shot, the receivers were conducted along a linear array of 8 at spacing of 0.25 m and the move step $\Delta d = 0.25$ m. Thus, 6 times of excitation were carried out on an entire measurement line.

In waveform acquisition work, The sensors were seismic receivers made by Geospace. Its heretic frequency was 4.5 Hz. The sampling rate was 31.25 μs. In views of that the buried depth of defects

Fig. 14. Real model of ballastless high-speed railway undertrack structure.

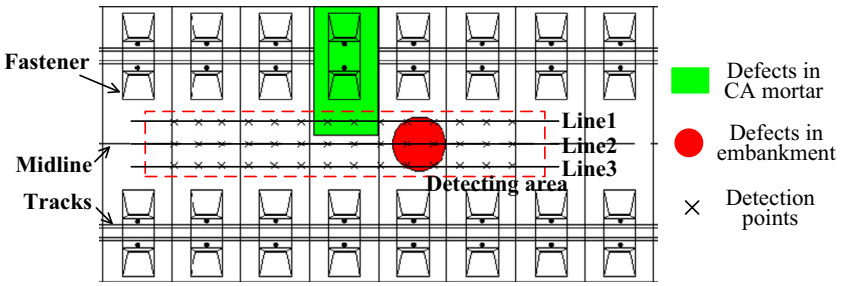

Fig. 15. Defects and measurement lines in real model.

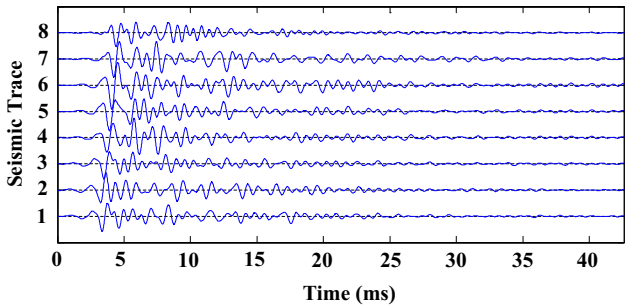

Fig. 16. Acquired waveforms (filtered) for one shot.

were relative shallow and less than 1 m, most of short-term dynamic load was used in FWI method. Also, the source waveforms had no effect on final results because of convolution algorithm. So manual hammer weight about 1.5 pounds was chosen as hypocenter in data acquisition. The hammer was vertically stroke and also vertical vibration signals were detected and recorded by a small seismograph. In view of the various noise in work field, especially the low-frequency signals, the acquired waveforms were filtered by band-pass of 500–4000 Hz. The acquired waveforms for one shot were shown in Fig. 16.

Before the inversion work, a proper initial model was important for its success rates. At first, the number of revealed parameters in model would be limited to reduce computational cost, so the Poisson's ratio and density for the entire model during inversion were kept constant.

Then, in order to obtain the S-wave velocity of concrete used in track slab, a frequency dispersion analysis was adopted on the acquired waveforms data, as Fig. 17 shows. The average phase velocity corresponding with the high frequency (3000–3500 Hz) was taken as the Rayleigh surface wave velocity of the first layer (track slab). Moreover, the Poisson's ratio of concrete was 0.2 according to the China National Standard 'Code for design of concrete structure'. Thus, the S-wave velocity of track slab was obtained by elastic assumption and equal to 1809 m/s. Also, the parameters of support plate in inversion work were same with track slab. The physical property parameters in model were listed in Table 2.

4.3. Inversion work

Mostly, 3D model required much more calculation cost than 2D model. Meanwhile, by appropriate waveforms pretreating work in mathematics, such as filtering, normalization, phase adjustment, 2D model was qualified for the FWI method in practical use. So to simplify the inversion work, 2D model was used here.

Table 2
Material parameters in inversion model.

Layers	Material name	ρ (kg/m^3)	v_s (m/s)	μ
Track slab	Concrete	2400	1809	0.2
CA mortar	CA mortar	1600	1500	0.3
Support plate	Concrete	2400	1809	0.2
Embankment	Gravel & sludge	2300	1600	0.25

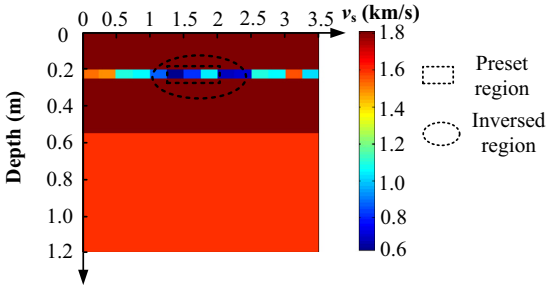

Fig. 18. S-wave profile of measurement Line 1.

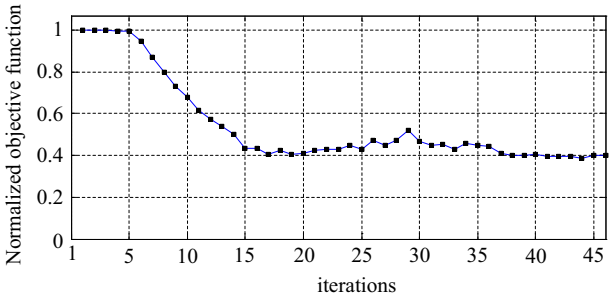

Fig. 19. Normalized values of objective function vary with iterations.

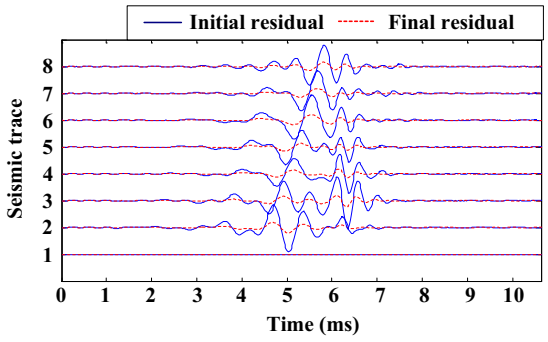

Fig. 20. Comparison between initial and final convolved residual data in model tests.

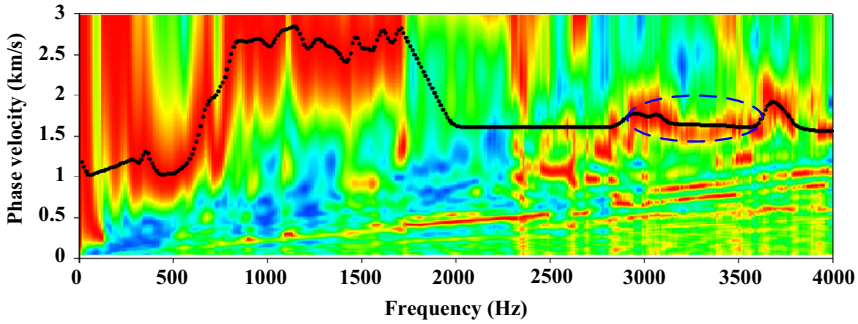

Fig. 17. Dispersion analysis for acquired waveforms.

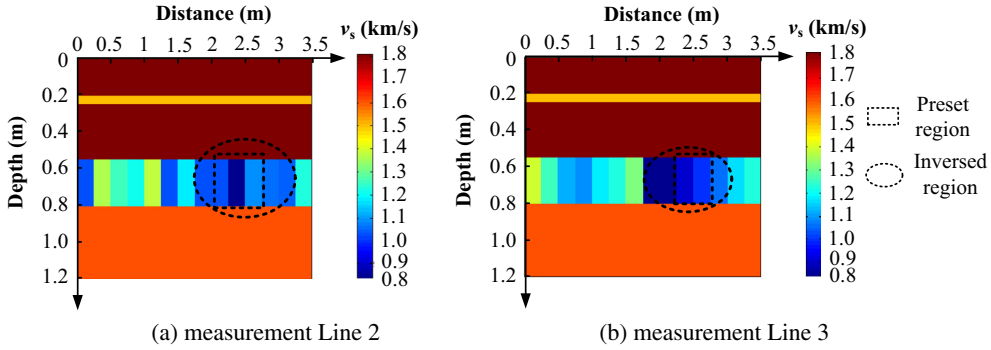

Fig. 21. S-wave profiles of measurement Line 2 and Line 3.

For the measurement Line 1, = we assumed that the parameters to be extracted were concentrated on the S-wave velocities of CA mortar. Similar with the numerical case, the initial values of S-wave velocities in CA mortar layer were all set as 1100 m/s at the beginning of inversion. Then, 46 iterations were performed. The S-wave profile of measurement Line 1 was shown in Fig. 18. The revealed defects in layer of CA mortar were located in the region from station 1.0 m to 2.5 m while the preset void was located in station from 1.25 to 2.0 m. It was observed that the location of defects revealed by the mentioned FWI method was generally consistent with the preset real model, but the revealed size was slightly enlarged.

The normalized values of objective function were reduced from 1.0 to 0.4, as shown in Fig. 19. The final residual data, which were convolved with corresponding reference trace, was declined and much smaller than initial residual data as presented in Fig. 20. Compared with the results of numerical case, the final residual data were still larger than those of 5% random noise corrupted data. The inversion errors could be possibly attributed to the following three reasons: Firstly, the high frequency noise could not be filtered. Secondly, the slight reflected waveforms generated at the free boundary of track slab. Thirdly, the discrepancy are still existed between real model and simplified model.

For the other two measurement lines, the defects were preset in embankment. So in the inversion work, the parameters to be extracted were concentrated in layer of embankment and its thickness was set as constant of 0.25 m. Then the inversion works were carried out similar with Line1. During the iterations, the parameter sensitiveness was obviously reduced because of the overlying strong reflection interface between track slab and CA mortar layer. The S-wave velocity profile of each measurement line revealed by our FWI method was shown in Fig. 21. It was observed that the locations of revealed defects agree with the preset while their sizes were enlarged by inversion. The errors were possibly attributed to the reduced parameter sensitiveness and disturbances mentioned in Line 1.

5. Conclusions

Base on the site investigation, the damage and defects are mainly concentrated in the weak layers of ballastless high-speed railway undertrack structure, especially the CA mortar and embankment. As a capable method for characterizing anomalies of low- and high- velocity zones, the full waveform inversion method is adopted into the quantitative detection on this ballastless undertrack structure. A time-domain FWI method is developed adopting quasi-linear method coupled with random search algorithm. Tikhonov regularization is used to alleviate the ill conditioned matrix. Also, by convolved with reference traces on observed data and forward response waveforms, the dependence on source is removed. Subsequently, this FWI method is tested by two numerical cases and the horizontal discontinuity of material is considered. In both of numerical cases, the preset damage regions in CA mortar and embankment are correctly revealed respectively. Also, the preset S-wave velocity structures are all recovered with 5% random noise. It is verified that the accuracy and convergence of this FWI method are reliable and available. Finally, this FWI method is applied on real data acquired from a full scale ballastless high-speed railway model. The results show that the inversion work successfully reveals the preset defects and damage in undertrack structure. Because of the disturbances and reduced parameter sensitiveness, the defects sizes are enlarged by inversion. Generally, this FWI method used in ballastless high-speed railway undertrack structure is practical and quantitative.

Acknowledgment

This work is financially supported by the National Natural Science Foundation of China (No. 11372180).

References

Berenger, J.P., 1994. A perfectly matched layer for the absorption of electromagnetic waves. J. Comput. Phys. 114 (2), 185–200.
Bunks, C., Saleck, F., Zaleski, S., 1995. Multi-scale seismic waveform inversion. Geophysics 60 (5), 1457–1473.
Brigham, J.C., Aquino, W., 2007. Surrogate-model accelerated random search algorithm for global optimization with applications to inverse material identification. Comput. Methods Appl. Mech. Eng. 196 (45), 4561–4576.
Brossier, R., Operto, S., Virieux, J., 2009. Seismic imaging of complex onshore structures by 2D elastic frequency-domain full-waveform inversion. Geophysics 74 (6), WCC105–WCC118.
Crase, E., Wideman, C., Noble, M., Tarantola, A., 1992. Nonlinear elastic waveform inversion of land seismic reflection data. J. Geophys. Res.: Solid Earth (1978–2012) 97 (B4), 4685–4703.
Cheong, S., Pyun, S., Shin, C.S., 2006. Two efficient steepest-descent algorithms for source signature-free waveform inversion: synthetic examples. J. Seismic Expl. 14 (4), 335.
Chew, W.C., Liu, Q.H., 1996. Perfectly matched layers for elastodynamics: a new absorbing boundary condition. J. Comput. Acoust. 4 (4), 341–359.
Cassidy, N.J., Millington, T.M., 2009. The application of finite-difference time-domain modelling for the assessment of GPR in magnetically lossy materials. J. Appl. Geophys. 67 (4), 296–308.
Fu, H.S., Han, B.A., 2004. A wavelet multiscale method for the inverse problems of a two-dimensional wave equation. Probl. Sci. Eng. 12, 643–656.
Feng, S.K., Takeshi, S., Che, A.L., 2009. Application of surface wave survey for nondestructive test of tunnel concrete lining. In: Proceedings of the 9th SEGJ International Symposium – Imaging and Interpretation, Sapporo, Japan, pp. 12–14.
Huang, X., Kelkar, M., 1996. Seismic inversion using heuristic combinatorial algorithm: a hybrid scheme. In: Proceedings of 66th International SEG Annual Conference. Denver: Society of Exploration Geo-physicists. vol. 119, pp. 125.
Lampe, J., Voss, H., 2013. Large-scale Tikhonov regularization of total least squares. J. Comput. Appl. Math. 238, 95–108.
O'Neill, A., Dentith, M., List, R., 2003. Full-waveform P-SV reflectivity inversion of surface waves for shallow engineering applications. Explor. Geophys. 34 (3), 158–173.

Romdhane, A., Grandjean, G., Brossier, R., Rejiba, F., Operto, S., Virieux, J., 2011. Shallow-structure characterization by 2D elastic full-waveform inversion. Geophysics 76 (3), R81–R93.
Smith, G.D., 1985. Numerical Solution of Partial Differential Equations: Finite Difference Methods. Oxford University Press.
Song, H.B., Matsubayashi, O., Kuramoto, S., 2003. Full waveform inversion of gas hydrate-related bottom simulating reflector. Chinese J. Geophys. 46 (1), 42–46.
Sheehan, J.R., Doll, W.E., Mandell, W.A., 2005. An evaluation of method sand available software for seismic refraction tomography analysis. J. Environ. Eng. Geophys. 10, 21–34.
Sheen, D.H., Tuncay, K., Bag, C.E., Ortoleva, P.J., 2006. Time domain Gauss–Newton seismic waveform inversion in elastic media. Geophys. J. Int. 167 (3), 1373–1384.
Tran, K.T., McVay, M., 2012. Site characterization using Gauss-Newton inversion of 2-D full seismic waveform in the time domain. Soil Dyn. Earthq. Eng. 43, 16–24.
Virieux, J., Operto, S., 2009. An overview of full-waveform inversion in exploration geophysics. Geophysics 74 (6), WCC1–WCC26.
Wang, S.H., 2005. The development of China's high-speed railway and its economic influence. J. Southwest Jiaotong Univ. (Soc. Sci.) 11 (5), 65–69.
Xu, X., Wu, J., Shen, J., 2006. Case study: application of GPR to detection of hidden dangers to underwater hydraulic structures. J. Hydraul. Eng. 132 (1), 12–20.
Yang, X.A., Gao, Y.L., 2004. GPR inspection for Shanghai-Nanjing railway tracked. Chinese J. Rock Mech. Eng. 23 (1), 116–119.
Yamanaka, H., 2005. Comparison of performance of heuristic search methods for phase velocity inversion in shallow surface wave method. J. Environ. Eng. Geophys. 10 (2), 163–173.